# Hybrid ^{18}F-Fluoroethyltyrosine PET and MRI with Perfusion to Distinguish Disease Progression from Treatment-Related Change in Malignant Brain Tumors: The Quest to Beat the Toughest Cases

Nathaniel J. Smith[1,2], Tristan K. Deaton[3], Wendy Territo[1], Brian Graner[1], Andrew Gauger[1], Scott E. Snyder[1], Michael L. Schulte[1], Mark A. Green[1], Gary D. Hutchins[1], and Michael C. Veronesi[1]

[1]School of Medicine, Indiana University, Indianapolis, Indiana; [2]Weldon School of Biomedical Engineering, Purdue University, West Lafayette, Indiana; and [3]Indiana University–Purdue University, Indianapolis, Indiana

Conventional MRI has important limitations when assessing for progression of disease (POD) versus treatment-related changes (TRC) in patients with malignant brain tumors. We describe the observed impact and pitfalls of implementing ^{18}F-fluoroethyltyrosine (^{18}F-FET) perfusion PET/MRI into routine clinical practice. **Methods:** Through expanded-access investigational new drug use of ^{18}F-FET, hybrid ^{18}F-FET perfusion PET/MRI was performed during clinical management of 80 patients with World Health Organization central nervous system grade 3 or 4 gliomas or brain metastases of 6 tissue origins for which the prior brain MRI results were ambiguous. The diagnostic performance with ^{18}F-FET PET/MRI was dually evaluated within routine clinical service and for retrospective parametric evaluation. Various ^{18}F-FET perfusion PET/MRI parameters were assessed, and patients were monitored for at least 6 mo to confirm the diagnosis using pathology, imaging, and clinical progress. **Results:** Hybrid ^{18}F-FET perfusion PET/MRI had high overall accuracy (86%), sensitivity (86%), and specificity (87%) for difficult diagnostic cases for which conventional MRI accuracy was poor (66%). ^{18}F-FET tumor-to-brain ratio static metrics were highly reliable for distinguishing POD from TRC (area under the curve, 0.90). Dynamic tumor-to-brain intercept was more accurate (85%) than SUV slope (73%) or time to peak (73%). Concordant PET/MRI findings were 89% accurate. When PET and MRI conflicted, ^{18}F-FET PET was correct in 12 of 15 cases (80%), whereas MRI was correct in 3 of 15 cases (20%). Clinical management changed after 88% (36/41) of POD diagnoses, whereas management was maintained after 87% (34/39) of TRC diagnoses. **Conclusion:** Hybrid ^{18}F-FET perfusion PET/MRI positively impacted the routine clinical care of challenging malignant brain tumor cases at a U.S. institution. The results add to a growing body of literature that ^{18}F-FET PET complements MRI, even rescuing MRI when it fails.

**Key Words:** malignant brain tumors; WHO CNS grade 3 or 4 glioma; glioblastoma; brain metastasis; amino acid PET; ^{18}F-fluoroethyltyrosine (FET) PET

Malignant gliomas of World Health Organization central nervous system grade 3 or 4 (adult-type diffuse glioma, ATDG) and brain metastases (BM) cause significant morbidity and mortality annually (1). Although management has improved, these malignancies remain difficult to treat. Even with specialized care, patients with glioblastoma have a mean survival of 15–20 mo with standard-of-care therapy, and only about 5% survive past 5 y (2). BMs are 10 times more common than primary malignant brain tumors, portend a poor prognosis, and continue rising in incidence (3,4).

Conventional MRI is the standard clinical imaging modality for managing brain tumors; however, it remains suboptimal for response assessment and treatment monitoring when distinguishing the progression of disease (POD) from treatment-related changes (TRCs) (5). MRI signal abnormalities lack biologic specificity, as T2-derived abnormalities reflect tissue water content, and contrast enhancement identifies regions of high blood–brain barrier permeability.

In MRI, perfusion-weighted imaging (PWI) indirectly measures malignancy by detecting neovascularity. Dynamic susceptibility contrast PWI captures signal loss within susceptibility-weighted sequences as paramagnetic gadolinium moves through tumor tissue (6). Dynamic contrast-enhanced PWI evaluates T1 relaxivity as gadolinium contrast medium passes through tissue (7). Although PWI techniques partially overcome conventional MRI limitations, reported clinical thresholds vary widely because of differences in acquisition protocols, scanner hardware, and overlapping tumor and normal-tissue parametric distributions (8–11).

To help overcome MRI's limitations, international working groups recommend amino acid PET imaging for complementary assessment of malignant brain tumors given superior tumor-to-background contrast (12–14). ^{18}F-fluoroethyltyrosine (^{18}F-FET) is the most commonly used amino acid radiotracer, providing a high diagnostic value for differentiating POD from TRC (15–18). PWI combined with ^{18}F-FET PET demonstrates increased sensitivity and specificity for delineating POD from TRC in malignant brain tumors, with hybrid ^{18}F-FET PET/MRI further increasing the accuracy (5,19,20).

We report the clinical application of hybrid ^{18}F-FET PET/MRI to patients with malignant brain tumors at a U.S. institution to

discern POD from TRC. This report provides additional evidence supporting the complementary nature of $^{18}$F-FET PET and MRI, reinforcing the European Association of Neurooncology/Response Assessment in Neurooncology (EANO/RANO) working group recommendations.

## MATERIALS AND METHODS

$^{18}$F-FET PET/MRI (3T Biograph mMR; Siemens) was performed for 80 adult patients with known ATDG ($n = 42$) or BM ($n = 38$). Advanced imaging discerned whether abnormalities in standard-of-care imaging corresponded to POD or TRC, with a 6-mo clinical follow-up (33 BM and 36 ATDG) or pathologic reference (5 BM and 6 ATDG) diagnosis. The institutional review board approved this study, and all subjects provided written informed consent for imaging with $^{18}$F-FET, which was prepared and clinically administered under expanded-access investigational-new-drug application 150883. Patients underwent standard cranial MRI, including 3-dimensional T1-weighted sequences before and after contrast medium, T2-weighted sequences, 3-dimensional fluid-attenuated inversion recovery sequences, diffusion-weighted imaging, apparent diffusion coefficient imaging, and susceptibility-weighted imaging. Patients received a half-and-half gadobutrol (Gadavist [Bayer]; 0.1 mL/kg of body weight) injection before dynamic susceptibility contrast MRI (repetition time, 1,600 ms; echo time, 30.0 ms; 90° flip angle; $1.7 \times 1.7 \times 4.0$ mm voxel size; 2,020-ms temporal resolution) and dynamic contrast-enhanced TWIST (time-resolved angiography with interleaved stochastic trajectories; Siemens) MRI (repetition time, 3.91 ms; echo time, 1.54 ms; dynamic temporal resolution, 2.70 s; 10° flip angle; $1.1 \times 1.1 \times 5.0$ mm voxel size). $^{18}$F-FET PET data were acquired in list mode from 0 to 40 min, concurrent with MRI acquisitions, allowing reconstruction as both single-frame late static images and a dynamic sequence for assessing regional radiopharmaceutical kinetics. $^{18}$F-FET (503–810 MBq) was administered as a bolus followed by a saline flush. Relatively high $^{18}$F-FET doses were used to enhance small-lesion (<10 mm) detection, with estimated critical organ doses remaining commensurate with standard clinical nuclear medicine procedures. Image analysis and interpretation followed the Society of Nuclear Medicine and European Association of Nuclear Medicine procedural recommendations for $^{18}$F-FET PET/MRI of brain tumors (14). $^{18}$F-FET analysis parameters included static (mean, maximum) and dynamic (slope, intercept, time-to-peak [TTP]) assessment for SUV and tumor-to-brain ratio (TBR) metrics (Fig. 1). PWI parameters included relative cerebral blood volume (rCBV), capillary permeability volume transfer constant ($K_{trans}$), and extravascular extracellular volume fraction. The Supplemental Methods contain more complete image acquisition, processing, and analysis details (supplemental materials are available at http://jnm.snmjournals.org) (7,14,21–32).

## RESULTS

### Patients

Eighty patients (47 men, 33 women) aged 17–77 y underwent $^{18}$F-FET PET/MRI. Most patients were at least 50 y old (75%) and were Caucasian (91%) (Table 1). Standard-of-care treatments included MRI-localized gross (36/80) and subtotal (16/80) resection; stereotactic radiosurgery (56/80); γ-knife (13/80) and whole-brain radiation (9/80); and temozolomide (32/80), bevacizumab (10/80), monoclonal antibody (28/80), DNA alkylation (15/80), and small-molecule kinase inhibitor (5/80) chemotherapies. Equivocal MRI examinations occurred a median of 188 d (range, 52–1,252 d) after the initiation of radiotherapy, and patients received a median 4 adjuvant doses (range, 0–12) of temozolomide. $^{18}$F-FET PET/MRI was performed a median of 10 mo (range, 2–95 mo) after radiation treatment, 9 mo (range, 1–76 mo) after surgery, and 38 d
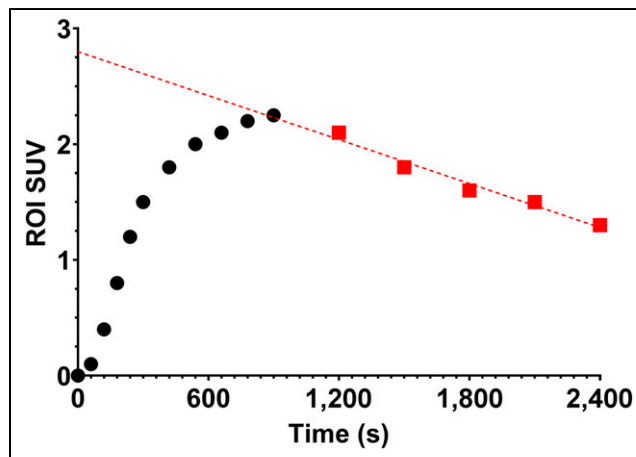


**FIGURE 1.** Dynamic slope and intercept estimation method. Regions of interest (ROIs) were located by neuroradiologist, and $SUV_{mean}$ was extracted for every frame in dynamic sequence. Linear regression to scan's final 20–40 min determined slope and intercept terms. Slope is reported in units of SUV/h. For TBR analysis, ROIs were normalized by contralateral reference tissue ROI for every frame in dynamic sequence with same linear regression procedure. TTP was estimated from SUV dynamic sequence global maximum.

(range, 10–394 d) after the latest MRI exam. The supplemental materials contains additional patient information.

Forty-two ATDG patients (30 glioblastoma, 2 grade 4 diffuse astrocytoma, and 10 grade 3 diffuse astrocytoma) underwent $^{18}$F-FET PET/MRI a median of 47 d after brain MRI with equivocal findings. Isocitrate dehydrogenase was wild type in 79% (33/42) patients, mutated in 19% (8/42) patients, and unknown in 1 patient. (6)-methylguanine-DNA methyltransferase was unmethylated in 43% (18/42) of patients, low-level methylated in 5% (2/42) of patients, methylated in 24% (10/42) of patients, hypermethylated in 14% (6/42) of patients, and unknown in 6 patients. Thirty-eight patients underwent $^{18}$F-FET PET/MRI to assess BM treatment response. Disease origins included lung in 47% (18/38), colon or rectum in

**TABLE 1**
Demographics for the 80 Study Patients

| Demographic | n |
| --- | --- |
| **Sex** | |
| Male | 47 (59%) |
| Female | 33 (41%) |
| **Age (y)** | |
| <40 | 6 (7.5%) |
| 40–49 | 14 (18%) |
| 50–59 | 29 (36%) |
| 60–69 | 25 (31%) |
| ≥70 | 6 (7.5%) |
| White/Caucasian* | 73 (91%) |
| Black/African American | 3 (4%) |
| Hispanic/Latinx | 2 (3%) |
| Asian | 2 (3%) |

*Denotes overrepresentation relative to overall US incidence.

## TABLE 2
### Institutional Performance with Hybrid $^{18}$F-FET PET/MRI

| Index | Overall | High-grade glioma | BM |
|---|---|---|---|
| Total patients | 80 | 42 | 38 |
| True-positive (true POD)* | 36 | 28 | 8 |
| True-negative (true TRC)* | 33 | 8 | 25 |
| False-positive* | 5 | 2 | 3 |
| False-negative* | 6 | 4 | 2 |
| Accuracy | 86% | 86% | 87% |
| Sensitivity | 86% | 88% | 80% |
| Specificity | 87% | 83% | 88% |
| Positive predictive value | 88% | 93% | 73% |
| Negative predictive value | 85% | 67% | 93% |
| Positive likelihood ratio | 6.5 | 4.4 | 7.5 |
| Negative likelihood ratio | 0.16 | 0.16 | 0.22 |
| False-positive rate | 13% | 20% | 11% |
| False-negative rate | 14% | 13% | 20% |

*Confirmed by 6 mo of follow-up.

Performance shown demonstrates overall clinical performance with integrating $^{18}$F-FET PET/MRI into care, using literature-based and institutional thresholds (rCBV > 3:1, $K_{trans}$ > 0.26, $TBR_{max}$ > 2.5) to assist in image-derived diagnosis.

5% (2/38), kidney in 13% (5/38), melanoma in 11% (4/38), breast in 18% (7/38), and thyroid in 3% (1/38) and were unspecified in 3% (1/38).

### Observed Performance of $^{18}$F-FET PET/MRI

Table 2 summarizes the institutional diagnostic performance of $^{18}$F-FET PET/MRI. The accuracy, sensitivity, and specificity were similar across all disease origins (~85%). Figure 2 demonstrates an example case with hybrid $^{18}$F-FET PET/PWI assisting to provide a diagnosis, and Supplemental Figures 1–4 provide examples of true-positive, true-negative, false-positive, and false-negative institutional diagnoses. Only 11 cases (14%) were misidentified in this study, 5 as false-positives and 6 as false-negatives. False-negative
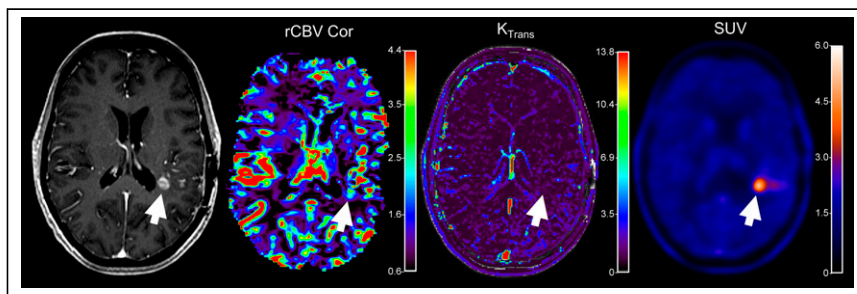


**FIGURE 2.** Patient with suspected recurrence of left parietal glioma (arrows) of World Health Organization central nervous system grade 4. Patient was initially evaluated with $^{18}$F-FET PET/MRI for increasing contrast-enhanced T1-weighted MRI findings posterior to left resection cavity. Dynamic contrast-enhanced $K_{trans}$ parameter met threshold for progression (0.38), but maximum rCBV value remained borderline (3.0). $^{18}$F-FET PET $TBR_{max}$ and $TBR_{mean}$ exceeded threshold at 2.75 and 2.3, respectively, supporting diagnosis of disease progression. Bevacizumab treatment was initiated, and enhancement and perfusion pattern improved on follow-up MRI, remaining stable for 2.5 y. Serial $^{18}$F-FET PET/MRI 2 y later remained stable.

diagnoses occurred nearly twice as frequently in ATDG patients (4/42, 9.5%) as in BM patients (2/38, 5.3%). Of the 11 misdiagnosed patients, 7 had a tumor volumes of less than 10 cm$^3$. Most mischaracterized lesions had increased in size from the previous MRI exam (7/11); 3 were stable, and 1 decreased in size.

Figure 3 and Supplemental Table 1 display the combined pathology receiver-operating-characteristic (ROC) performance for all perfusion MRI, TBR normalized $^{18}$F-FET PET/MRI uptake, and standardized $^{18}$F-FET PET/MRI uptake parameters. The supplemental materials contain replicate ROC analyses stratified by disease origin (BM or ATDG), optimized cutoff thresholds, performance characteristics, and statistical justification. Increasing tumor volume on conventional MRI was only 60% (33/55) predictive of POD, whereas stagnant or receding MRI tumor volume was 64% (16/25) predictive of TRC. Overall, $^{18}$F-FET PET/MRI metrics met or exceeded the diagnostic performance of perfusion MRI metrics. For combined ATDG and BM patients, maximum, mean, and intercept TBR metrics ($TBR_{max}$, $TBR_{mean}$, and $TBR_{intercept}$, respectively) generated area-under-the-ROC-curve (AUC) performance at or above 0.90 (Table 3). Institutional accuracy values mirrored the performance of these 3 metrics within 2% across all disease origins (BM or ATDG). In contrast, no perfusion-weighted MRI metric demonstrated an accuracy above 76%.

When directly compared, $TBR_{max}$, $TBR_{mean}$, and $TBR_{intercept}$ performed significantly better than $K_{trans}$ and rCBV (Fig. 4; Table 4). The optimal perfusion-weighted MRI POD threshold (rCBV > 3.85) would have led to 10 false-positive and 9 false-negative mischaracterizations for this cohort without $^{18}$F-FET PET. In these instances, 7 false-positives and 5 false-negatives would have been corrected by combination with the $TBR_{max}$ threshold of more than 2.69 or the $TBR_{mean}$ threshold of more than 2.16. Alternatively, if a $TBR_{max}$ of more than 2.69 was the sole diagnostic metric, 7 false-negative and 3 false-positive cases would have occurred, and only 3 of the false-negative diagnoses would have been corrected by the rCBV threshold of more than 3.85.

When stratified by disease origin, select dynamic $^{18}$F-FET PET/MRI metrics generated strong retrospective performance. Slope TBR metrics ($TBR_{slope}$) were 95% (36/38) accurate with an AUC of 0.97 for BM patients (Supplemental Fig. 5; Supplemental Table 2), and intercept SUV metrics ($SUV_{intercept}$) were 95% (40/42) accurate with an AUC of 0.96 for ATDG patients (Supplemental Fig. 6; Supplemental Table 3). Of the 5 BM patients who were incorrectly diagnosed, 4 had $TBR_{slope}$ values that were consistent with their correct diagnosis. Perfusion-weighted MRI parameters yielded up to 90% (38/42) accuracy for ATDG patients, and 5 of 6 of the misdiagnosed ATDG patients had $K_{trans}$ values and extravascular extracellular volume fractions consistent with their correct diagnosis. Further details on all patient disease characteristics, treatments, and imaging parameters can be found in Supplemental Tables 4–11. Supplemental Table 12 includes a small subset analysis of interrater reliability for PWI parameters, indicating strong correspondence between readers for $K_{trans}$ and rCBV.

### DISCUSSION

This study demonstrated the utility of hybrid $^{18}$F-FET PET/MRI with PWI in
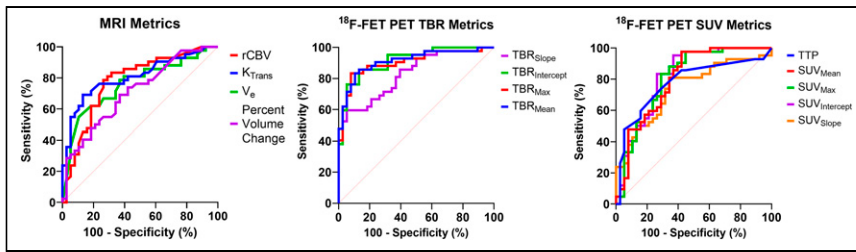
**FIGURE 3.** ROC curve analysis of perfusion-weighted MRI and $^{18}$F-FET PET/MRI. Sensitivity was calculated as ratio of detected cases to all POD cases, and specificity was calculated as ratio of detected cases to all TRC cases. MRI metrics include rCBV, $K_{trans}$, and extravascular extracellular volume fraction ($V_e$). PET metrics included TBR, SUV, and TTP concentration. Dashed red line represents nondiagnostic test performance. Associated ROC quantitative analyses are in Table 3.

routine clinical medicine, applied across various primary and secondary disease origins, treatment regimens, and diagnostic timelines. Despite the patient heterogeneity, reported PWI and $^{18}$F-FET PET performance were consistent with the literature. For ATDG patients, our rCBV (DSC MRI) sensitivity of 84%, specificity of 80%, and AUC of 0.88 were within the confidence bounds of a recent metaanalysis released by Fu et al. (33). Additionally, the $K_{trans}$ (dynamic contrast-enhanced MRI) specificity of 80% and AUC of 0.88 for ATDG patients were within the confidence bounds of a metaanalysis released by Taylor et al., whereas our reported sensitivity was slightly higher, at 94% (34). Evidence for PWI is limited in BM patients, but Cicone et al. reported an rCBV accuracy of 76% and AUC within 0.65–0.96, which complement our 76% accuracy and AUC of 0.74 (35).

The complementary nature of perfusion-weighted MRI and amino acid PET uptake imaging improved clinician confidence compared with MRI alone. Importantly, when dynamic susceptibility contrast or dynamic contrast-enhanced MRI is suboptimal or nondiagnostic, $^{18}$F-FET PET still supports high clinician diagnostic confidence because it resists PWI failure (36). Because interreader qualitative assessment varies with PWI alone (37), complementary imaging enables a more robust diagnostic outcome. Previous studies have advocated for sequential PWI and $^{18}$F-FET PET in glioma evaluation due to a 100% reported positive predictive value for rCBV, but our reported 93% positive predictive value for rCBV did not exceed that of TBR$_{mean}$ or TBR$_{max}$ (96% and 97%, respectively) (38). $^{18}$F-FET PET parameters also provided higher accuracy (TBR$_{mean}$, 86%; TBR$_{max}$, 88%) than rCBV (83%), supporting the use of simultaneous hybrid imaging, when available.

In this study, diagnostic accuracy was 89% (58/65) when PWI and $^{18}$F-FET PET findings were concordant. When discordant, $^{18}$F-FET PET indicated the correct diagnosis in 80% (12/15) of patients. However, 45% (5/11) of the false diagnoses occurred when hybrid imaging was discordant. In the 20% (3/15) of discordant imaging findings for which PWI indicated the correct diagnosis, $^{18}$F-FET PET failed to detect POD. Overall, the institutional diagnostic accuracy mirrors that of $^{18}$F-FET PET alone. Hybrid imaging exceeded the performance of perfusion MRI alone, but the impact of other useful MRI techniques, such as diffusion-weighted imaging, MR spectroscopy, and kurtosis imaging, was not evaluated in this study (19,39–41).

Our institution's $^{18}$F-FET PET criteria included a TBR$_{max}$ of more than 2.5 and a TBR$_{mean}$ of more than 2.0, guided by publications cited in the EANO/RANO update (14). Calculated glioma

**TABLE 3**
Retrospective ROC-Optimized Thresholds and Analysis Results in All Patients (38 TRC, 42 POD) (for Fig. 3)

| Modality | Parameter | Cutoff (%) | SN (%) | SP (%) | ACC (%) | PPV (%) | NPV (%) | AUC | 95% CI | Adjusted $P$ |
|---|---|---|---|---|---|---|---|---|---|---|
| MRI | Volume change | >13.5 | 69 | 63 | 66 | 67 | 65 | 0.71 | 0.60–0.82 | <0.01 |
| Perfusion MRI | rCBV | >3.85 | 79 | 74 | 76 | 77 | 76 | 0.78 | 0.67–0.88 | <0.0001 |
| | $K_{trans}$ | >0.58 | 76 | 76 | 76 | 78 | 74 | 0.81 | 0.71–0.90 | <0.0001 |
| | $V_e$ | >0.98 | 62 | 82 | 71 | 79 | 66 | 0.76 | 0.65–0.87 | <0.0001 |
| $^{18}$F-FET PET (TBR) | TBR$_{slope}$ | <−0.69 | 67 | 79 | 73 | 78 | 68 | 0.83 | 0.74–0.92 | <0.0001 |
| | TBR$_{intercept}$ | >2.39 | 83 | 87 | 85 | 88 | 83 | 0.91 | 0.85–0.98 | <0.0001 |
| | TBR$_{max}$ | >2.69 | 83 | 92 | 88 | 92 | 83 | 0.90 | 0.84–0.97 | <0.0001 |
| | TBR$_{mean}$ | >2.16 | 86 | 87 | 86 | 88 | 85 | 0.91 | 0.85–0.98 | <0.0001 |
| $^{18}$F-FET PET (SUV) | SUV$_{slope}$ | <0.24 | 81 | 66 | 73 | 71 | 75 | 0.74 | 0.63–0.85 | <0.001 |
| | SUV$_{intercept}$ | >2.07 | 83 | 74 | 79 | 78 | 80 | 0.82 | 0.72–0.91 | <0.0001 |
| | SUV$_{max}$ | >2.42 | 83 | 71 | 76 | 76 | 77 | 0.81 | 0.71–0.91 | <0.0001 |
| | SUV$_{mean}$ | >2.01 | 81 | 66 | 74 | 72 | 76 | 0.80 | 0.70–0.90 | <0.0001 |
| | TTP | <1,800 | 74 | 71 | 73 | 74 | 71 | 0.78 | 0.67–0.88 | <0.0001 |

SN = sensitivity; SP = specificity; ACC = accuracy; PPV = positive predictive value; NPV = negative predictive value; $V_e$ = extravascular extracellular volume fraction.

Significance is adjusted for multiple comparisons using Benjamini–Hochberg method and tests for AUC > 0.5. All metrics tested as significant. Cutoffs were calculated by optimizing geometric mean of sensitivity and specificity for ROC curve.
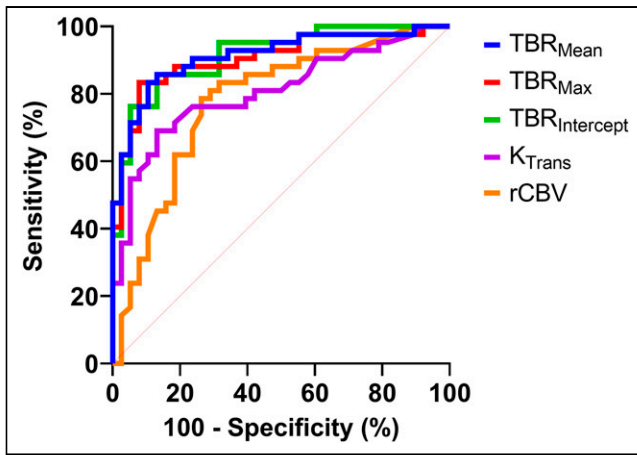
**FIGURE 4.** ROC curve performance comparison for select perfusion-weighted MRI and $^{18}$F-FET PET parameters. Sensitivity was calculated as ratio of detected cases to all POD cases, and specificity was calculated as ratio of detected cases to all TRC cases. MRI metrics include rCBV and $K_{trans}$. PET metrics included $TBR_{intercept}$, $TBR_{max}$, and $TBR_{mean}$. Dashed red line represents nondiagnostic test performance. Associated comparative tests are in Table 4.

thresholds included a $TBR_{max}$ of more than 2.42 and a $TBR_{mean}$ of more than 2.16, in support of the criteria. Individually, these static $^{18}$F-FET PET TBR parameters achieved 86%–88% diagnostic accuracy, 84%–88% sensitivity, and 90% specificity, consistent with other reports (17,39). For BM, our diagnostic accuracy with $TBR_{max}$ approximates literature values, but with an elevated threshold of 2.79 relative to the 2.55 literature threshold (15,16). POD prevalence was only 26% (10/38) in our BM patients, which could generate a biased threshold estimate. Combined, our data support a $TBR_{max}$ threshold of 2.69 (88% accuracy, 83% sensitivity,

**TABLE 4**
ROC Comparison of Select Perfusion-Weighted MRI and $^{18}$F-FET PET/MRI Metrics (for Fig. 4)

| Metrics compared | Metric 1 AUC | Metric 2 AUC | Adjusted P |
|---|---|---|---|
| $TBR_{intercept}$ vs. rCBV | 0.9148 | 0.7785 | 0.024* |
| $TBR_{mean}$ vs. rCBV | 0.9123 | 0.7785 | 0.015* |
| $TBR_{max}$ vs. rCBV | 0.9041 | 0.7785 | 0.013* |
| $TBR_{intercept}$ vs. $K_{trans}$ | 0.9148 | 0.8058 | 0.025* |
| $TBR_{mean}$ vs. $K_{trans}$ | 0.9123 | 0.8058 | 0.026* |
| $TBR_{max}$ vs. $K_{trans}$ | 0.9041 | 0.8058 | 0.028* |
| $K_{trans}$ vs. rCBV | 0.8058 | 0.7785 | 0.310 (NS) |

*$P < 0.05$.
NS = not significant.
P values are calculated using Hanley ROC comparison method and adjusted for multiple comparisons using Benjamini–Hochberg method. Significance tests are for overperformance of metric 1 relative to metric 2. Evaluated over entire 80-patient sample, listed TBR metrics demonstrate superior performance in AUC compared with $K_{trans}$ and rCBV. No significant difference in performance exists between rCBV (dynamic susceptibility contrast MRI) and $K_{trans}$ (dynamic contrast-enhanced MRI).

92% specificity) across all disease origins. Our threshold exceeds the suggested EANO/RANO criteria of 2.5 (84% accuracy, 86% sensitivity, 82% specificity), reflecting a blend of the BM and ATDG stratified criteria. Compared with international recommendations, our threshold improves the overall accuracy for our patients, but at the cost of slightly reduced sensitivity and an increased false-negative rate.

Guidelines for ATDG and BM evaluation recommend the use of static and dynamic $^{18}$F-FET PET analysis (13,14), promoting slope SUV metrics ($SUV_{slope}$) and TTP as the most accurate dynamic metrics. Although $SUV_{slope}$ and TTP demonstrated strong performance for BM and ATDG, with our results matching literature accuracy (39), our data suggest the need for an origin-specific diagnostic approach. For ATDG, $SUV_{intercept}$ enabled a 95% diagnostic accuracy, with an AUC greater than the TTP and $SUV_{slope}$ (Supplemental Table 3). Because the $SUV_{intercept}$ varies with the TTP, $SUV_{slope}$, and the absolute SUV scaling of the time–activity curve, we hypothesize that performance characteristics can be attributed to this multifactorial diagnostic combination. For BM, $TBR_{slope}$ enabled a 95% diagnostic accuracy (Supplemental Table 2), outperforming $SUV_{slope}$. Because TBR metrics normalize the SUV signal to a contralateral reference region, we posit that $TBR_{slope}$ achieves high accuracy by reducing the impact of regional uptake differences and patient weight variability.

$^{18}$F-FET prompted false-negative conclusions more frequently when the lesion was less than 10 cm$^3$ in volume (Supplemental Fig. 4), consistent with other reports indicating the importance of suprathreshold tumor volumes (42). Partial-volume artifacts can dilute the $^{18}$F-FET signal from small lesions, obscuring them with adjacent brain signals. To address this, serial $^{18}$F-FET PET/MRI may enhance subclinical lesion interpretation when compared with single-session $^{18}$F-FET PET/MRI and periodic follow-up PWI.

This study demonstrates the value of clinical $^{18}$F-FET PET/MRI; however, there are still limitations to its clinical use. Clinical scans are inconsistent in their posttreatment timing and are subject to treatment heterogeneity. This study is also susceptible to referral bias, omitting cases in which a prior MRI exam sufficiently established a definitive diagnosis, as evidenced by the low diagnostic performance of contrast-enhanced MRI lesion volume change relative to other investigated parameters (Table 3). However, this implicit focus on challenging case referrals is consistent with other reports in the literature and with the common clinical indications for $^{18}$F-FET PET (43). Additionally, this study was limited in sample size for stratification by disease type. When assessing ATDG alone, there was an asymmetrically higher number of cases of POD (76%, 32/42) than of METs (24%, 10/42). Conversely, there were fewer METs with POD (26%, 10/38) than with TRC (74%, 28/38). Although most analyses were considered in aggregate, the supplemental materials stratified by disease type did not have balanced outcomes and should be interpreted cautiously.

**CONCLUSION**

This study demonstrates the overall benefit of implementing hybrid $^{18}$F-FET PET/MRI for patients with malignant brain tumors when conventional MRI and PWI were equivocal for discerning disease progression from nonmalignant treatment changes. Sample size limitations and the subjective nature of regional analysis may limit the generalizability of the study findings; however, this study provides a benchmark for prospective analyses and establishes a framework through which $^{18}$F-FET PET/MRI may be clinically introduced.

---

**KEY POINTS**

**QUESTION:** What is the clinical impact of perfusion ^{18}F-FET PET/MRI on assessing posttreatment brain malignancies?

**PERTINENT FINDINGS:** TBR metrics can distinguish posttreatment disease progression from treatment-related change with high accuracy.

**IMPLICATIONS FOR PATIENT CARE:** ^{18}F-FET PET/MRI improves clinician diagnostic confidence and informs timely, appropriate treatment modifications.

---

## REFERENCES

1. Miller KD, Ostrom QT, Kruchko C, et al. Brain and other central nervous system tumor statistics, 2021. *CA Cancer J Clin.* 2021;71:381–406.
2. Stupp R, Taillibert S, Kanner AA, et al. Maintenance therapy with tumor-treating fields plus temozolomide vs temozolomide alone for glioblastoma: a randomized clinical trial. *JAMA.* 2015;314:2535–2543.
3. Nieblas-Bedolla E, Zuccato J, Kluger H, Zadeh G, Brastianos PK. Central nervous system metastases. *Hematol Oncol Clin North Am.* 2022;36:161–188.
4. Ostrom QT, Wright CH, Barnholtz-Sloan JS. Chapter 2: brain metastases—epidemiology. In: Schiff D, van den Bent MJ, eds. *Handbook of Clinical Neurology.* Vol 149. Elsevier; 2018:27–42.
5. Stopa BM, Juhász C, Mittal S. Comparison of amino acid PET to advanced and emerging MRI techniques for neurooncology imaging: a systematic review of the recent studies. *Mol Imaging.* 2021;2021:8874078.
6. Lev MH, Ozsunar Y, Henson JW, et al. Glial tumor grading and outcome prediction using dynamic spin-echo MR susceptibility mapping compared with conventional contrast-enhanced MR: confounding effect of elevated rCBV of oligodendroglimoas. *Am J Neuroradiol.* 2004;25:214–221.
7. Tofts PS, Brix G, Buckley DL, et al. Estimating kinetic parameters from dynamic contrast-enhanced $t_1$-weighted MRI of a diffusable tracer: standardized quantities and symbols. *J Magn Reson Imaging.* 1999;10:223–232.
8. Shukla-Dave A, Obuchowski NA, Chenevert TL, et al. Quantitative imaging biomarkers alliance (QIBA) recommendations for improved precision of DWI and DCE-MRI derived biomarkers in multicenter oncology trials. *J Magn Reson Imaging.* 2019;49:e101–e121.
9. Bell LC, Semmineh N, An H, et al. Evaluating the use of rCBV as a tumor grade and treatment response classifier across NCI quantitative imaging network sites: part II of the DSC-MRI digital reference object (DRO) challenge. *Tomography.* 2020;6:203–208.
10. Wang L, Wei L, Wang J, et al. Evaluation of perfusion MRI value for tumor progression assessment after glioma radiotherapy. *Medicine (Baltimore).* 2020;99:e23766.
11. Patel P, Baradaran H, Delgado D, et al. MR perfusion-weighted imaging in the evaluation of high-grade gliomas after treatment: a systematic review and metaanalysis. *Neuro Oncol.* 2017;19:118–127.
12. Albert NL, Weller M, Suchorska B, et al. Response assessment in neuro-oncology working group and European Association for neuro-oncology recommendations for the clinical use of PET imaging in gliomas. *Neuro Oncol.* 2016;18:1199–1208.
13. Galldiks N, Langen K-J, Albert NL, et al. PET imaging in patients with brain metastasis: report of the RANO/PET group. *Neuro Oncol.* 2019;21:585–595.
14. Law I, Albert NL, Arbizu J, et al. Joint EANM/EANO/RANO practice guidelines/SNMMI procedure standards for imaging of gliomas using PET with radiolabelled amino acids and [18F]FDG: version 1.0. *Eur J Nucl Med Mol Imaging.* 2019;46:540–557.
15. Galldiks N, Stoffels G, Filss CP, et al. Role of O-(2-[18F-fluoroethyl)-ʟ-tyrosine PET for differentiation of local recurrent brain metastasis from radiation necrosis. *J Nucl Med.* 2012;53:1367–1374.
16. Ceccon G, Lohmann P, Stoffels G, et al. Dynamic O-(2-[18F-fluoroethyl)-L-tyrosine positron emission tomography differentiates brain metastasis recurrence from radiation injury after radiotherapy. *Neuro Oncol.* 2017;19:281–288.
17. de Zwart PL, van Dijken BRJ, Holtman GA, et al. Diagnostic accuracy of PET tracers for the differentiation of tumor progression from treatment-related changes in high-grade glioma: a systematic review and metaanalysis. *J Nucl Med.* 2020;61:498–504.
18. Henriksen OM, Hansen AE, Muhic A, et al. Diagnostic yield of simultaneous dynamic contrast-enhanced magnetic resonance perfusion measurements and [18F]FET PET in patients with suspected recurrent anaplastic astrocytoma and glioblastoma. *Eur J Nucl Med Mol Imaging.* 2022;49:4677–4691.
19. Sogani SK, Jena A, Taneja S, et al. Potential for differentiation of glioma recurrence from radionecrosis using integrated ^{18}F-fluoroethyl-L-tyrosine (FET) positron emission tomography/magnetic resonance imaging: a prospective evaluation. *Neurol India.* 2017;65:293–301.
20. Pyka T, Hiob D, Preibisch C, et al. Diagnosis of glioma recurrence using multiparametric dynamic ^{18}F-fluoroethyl-tyrosine PET-MRI. *Eur J Radiol.* 2018;103:32–37.
21. Rosen BR, Belliveau JW, Vevea JM, Brady TJ. Perfusion imaging with NMR contrast agents. *Magn Reson Med.* 1990;14:249–265.
22. Pöpperl G, Götz C, Rachinger W, Gildehaus F-J, Tonn J-C, Tatsch K. Value of O-(2-[18F]fluoroethyl)-L-tyrosine PET for the diagnosis of recurrent glioma. *Eur J Nucl Med Mol Imaging.* 2004;31:1464–1470.
23. Louis DN, Perry A, Reifenberger G, et al. The 2016 World Health Organization classification of tumors of the central nervous system: a summary. *Acta Neuropathol (Berl).* 2016;131:803–820.
24. Louis DN, Perry A, Wesseling P, et al. The 2021 WHO classification of tumors of the central nervous system: a summary. *Neuro Oncol.* 2021;23:1231–1251.
25. McHugh ML. Interrater reliability: the kappa statistic. *Biochem Med (Zagreb).* 2012;22:276–282.
26. Shrout PE, Fleiss JL. Intraclass correlations: uses in assessing rater reliability. *Psychol Bull.* 1979;86:420–428.
27. Youden WJ. Index for rating diagnostic tests. *Cancer.* 1950;3:32–35.
28. Clopper CJ, Pearson ES. The use of confidence or fiducial limits illustrated in the case of the binomial. *Biometrika.* 1934;26:404–413.
29. Hanley JA, McNeil BJ. The meaning and use of the area under a receiver operating characteristic (ROC) curve. *Radiology.* 1982;143:29–36.
30. Hanley JA, McNeil BJ. A method of comparing the areas under receiver operating characteristic curves derived from the same cases. *Radiology.* 1983;148:839–843.
31. Benjamini Y, Hochberg Y. Controlling the false discovery rate: a practical and powerful approach to multiple testing. *J R Stat Soc B.* 1995;57:289–300.
32. Benjamini Y, Heller R, Yekutieli D. Selective inference in complex research. *Philos Trans A Math Phys Eng Sci.* 2009;367:4255–4271.
33. Fu R, Szidonya L, Barajas RF Jr, Ambady P, Varallyay C, Neuwelt EA. Diagnostic performance of DSC perfusion MRI to distinguish tumor progression and treatment-related changes: a systematic review and meta-analysis. *Neurooncol Adv.* 2022;4:vdac027.
34. Taylor C, Ekert JO, Sefcikova V, Fersht N, Samandouras G. Discriminators of pseudoprogression and true progression in high-grade gliomas: a systematic review and meta-analysis. *Sci Rep.* 2022;12:13258.
35. Cicone F, Minniti G, Romano A, et al. Accuracy of F-DOPA PET and perfusion-MRI for differentiating radionecrotic from progressive brain metastases after radiosurgery. *Eur J Nucl Med Mol Imaging.* 2015;42:103–111.
36. Overcast WB, Davis KM, Ho CY, et al. Advanced imaging techniques for neuro-oncologic tumor diagnosis, with an emphasis on PET-MRI imaging of malignant brain tumors. *Curr Oncol Rep.* 2021;23:34.
37. Zakhari N, Taccone M, Torres C, et al. Qualitative assessment of advanced MRI in post-treatment high grade gliomas follow up: do we agree? *Can Assoc Radiol J.* 2022;73:187–193.
38. Steidl E, Langen K-J, Hmeidan SA, et al. Sequential implementation of DSC-MR perfusion and dynamic [18F]FET PET allows efficient differentiation of glioma progression from treatment-related changes. *Eur J Nucl Med Mol Imaging.* 2021;48:1956–1965.
39. Brendle C, Maier C, Bender B, et al. Impact of ^{18}F-FET PET/MR on clinical management of brain tumor patients. *J Nucl Med.* 2022;63:522–527.
40. Dang H, Zhang J, Wang R, et al. Glioblastoma recurrence versus radiotherapy injury: combined model of diffusion kurtosis imaging and ^{11}C-MET using PET/MRI may increase accuracy of differentiation. *Clin Nucl Med.* 2022;47:e428–e436.
41. D'Amore F, Grinberg F, Mauler J, et al. Combined ^{18}F-FET PET and diffusion kurtosis MRI in posttreatment glioblastoma: differentiation of true progression from treatment-related changes. *Neurooncol Adv.* 2021;3:vdab044.
42. Paprottka KJ, Kleiner S, Preibisch C, et al. Fully automated analysis combining [18F]-FET-PET and multiparametric MRI including DSC perfusion and APTw imaging: a promising tool for objective evaluation of glioma progression. *Eur J Nucl Med Mol Imaging.* 2021;48:4445–4455.
43. Heinzel A, Dedic D, Galldiks N, et al. Two decades of brain tumour imaging with O-(2-[18F]fluoroethyl)-L-tyrosine PET: the Forschungszentrum Jülich experience. *Cancers (Basel).* 2022;14:3336.